TCM Control in High-frequency Inverter Without Bottom Current Detection

Rintaro Kusui
Dept. of Science of Technology Innovation
Nagaoka University of Technology
Nagaoka, Japan
kusui@stn.nagaokaut.ac.jp

Shogo Hiroike
Dept. of Electrical, Electronics and Information Engineering
Nagaoka University of Technology
Nagaoka, Japan
s223141@stn.nagaokaut.ac.jp

Takumi Iwamoto
Dept. of Science of Technology Innovation
Nagaoka University of Technology
Nagaoka, Japan
s225057@stn.nagaokaut.ac.jp

Hiroki Watanabe
Dept. of Electrical, Electronics and Information Engineering
Nagaoka University of Technology
Nagaoka, Japan
hwatanabe@vos.nagaokaut.ac.jp

Yuki Nakata
Dept. of Social Design Engineering
National Institute of Technology Kochi College
Kochi, Japan
nakata@ee.kochi-ct.ac.jp

Jun-ichi Itoh
Dept. of Science of Technology Innovation
Nagaoka University of Technology
Nagaoka, Japan
itoh@vos.nagaokaut.ac.jp

***Abstract*— This paper proposes a method to drive the inductor current in Triangular Current Mode (TCM) without detecting the bottom current. Detecting the bottom current is difficult at high switching frequencies due to the bandwidth limitations of the shunt resistor and peripheral circuits. The proposed method achieves TCM operation by calculating the turn-on and turn-off times. However, if the bottom current is not detected, current errors may occur due to parameter errors and voltage fluctuations within a switching cycle. The proposed method compensates for the current error by proportional control based on the detected filter inductor current. The operation of the proposed method is verified through simulation and experiment. The experimental results confirm that the grid-tied inductor current operates in TCM and that the filter inductor current follows the reference value. The total harmonic distortion (THD) of the filter inductor current under this condition is 2.8%.**

Keywords—high-frequency DC-AC converter, triangle current mode, bottom current detection

I. INTRODUCTION

In recent years, the growing adoption of renewable energy and electric vehicles has increased the demand for power converters with high power density [1]. Conventional development methods for power electronic systems require a wide range of expertise—such as circuit design, thermal management, noise mitigation, and software development—resulting in prolonged development times and high costs. The Universal Smart Power Module (USPM) has been proposed. USPM enables the construction of power electronic systems simply by combining pre-designed modules and developing software for a master controller [2-3]. Each USPM module integrates a main power circuit, gate driver, controller, detection circuit, and noise filter. The controller has a SoC-FPGA and a high-speed sampling ADC [4]. As a result, engineers can develop various power electronic systems by combining modules without requiring extensive specialized knowledge[5-7]. However, to further promote the widespread use of USPM, increasing the power density of power conversion circuits remains a critical challenge.

Increasing the switching frequency is an effective approach to enhancing the power density of power converters [8][9]. While higher switching frequencies enable the use of smaller passive components, they also lead to increased switching losses. Reference [10][11] proposes that triangular current mode (TCM) reduces switching losses. TCM achieves zero-voltage switching (ZVS) by employing a small inductor and variable frequency control. ZVS requires a negative current to discharge the parasitic capacitance of the switching device during the dead time. Consequently, current sensing must be performed with a bandwidth significantly higher than the switching frequency. This requirement poses a challenge for applying TCM to high-frequency inverters operating in the MHz range.

This paper proposes a TCM control method that does not require high-speed detection of the bottom current. The proposed method achieves the desired average current and the bottom current necessary for ZVS by calculating the turn-on and turn-off times of the switching devices. However, fluctuations in input/output voltages during the switching cycle and inductance errors may cause errors in the inductor current. The proposed method introduces an LCL filter at the output stage of the inverter and compensates for output current errors through feedback control of the filter inductor current. As a result, TCM operation is achieved without high-speed current detection or high-bandwidth controllers. The remainder of this paper presents simulation results at a minimum switching frequency of 2 MHz and experimental results at 100 kHz to verify its effectiveness.

II. PROPOSED TCM CONTROL METHOD

A. Circuit configuration

Figure 1 shows the circuit configuration of a full-bridge inverter employing the proposed method. The main circuit consists of a single-phase inverter and an LCL filter. The grid-tied inductor is designed such that the switching frequency

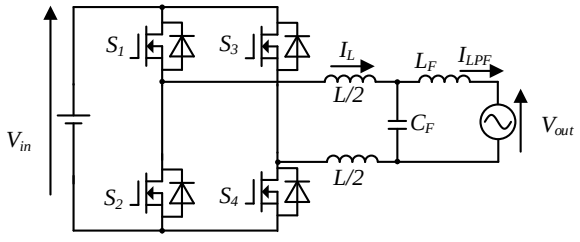

Fig. 1. Circuit configuration.

reaches its minimum when the current is at its maximum. The filter inductor and capacitor are designed so that the cutoff frequency is approximately 1/10 of the minimum switching frequency. The filter inductor current is detected by a current sensor instead of a shunt resistor because the proposed method does not require high-speed current sensing.

B. Proposed TCM Control

Figure 2 illustrates the operating modes of a single-phase inverter. The inverter employs four modes to control the load current while preventing short-circuit conditions in the power supply and open-circuit conditions in current-source loads.

In Mode 1, switches S_1 and S_4 are turned on, and the inverter outputs the DC voltage V_{in}. The grid-tied inductor is applied with the voltage difference between V_{in} and the filter capacitor voltage v_c (i.e., $V_{in} - v_c$). The capacitor voltage vc is approximately equal to the output voltage, and the output voltage is lower than Vin. Therefore, the inductor current increases.

In Modes 2 and 4, upper- or lower-arm switches are turned on simultaneously, resulting in a zero output voltage. In this mode, an inductor voltage is $-v_c$, causing the inductor current to either increase or decrease depending on the polarity of v_c.

In Mode 3, switches S_2 and S_3 are turned on, and the inverter outputs $-V_{in}$. As a result, an inductor voltage is $-V_{in} - v_c$, leading to a decrease in inductor current.

Figure 3 shows the inductor current waveform operating in TCM when the output voltage v_{out} is positive. The inductor current increases to the peak current I_{peak} during Mode 1 and then decreases to the bottom current I_{bot} during Mode 2 or 3, assuming unipolar modulation. The bottom current I_{bot} is set sufficiently low to enable ZVS operation.

The average value of inductor current i_{avg} is expressed as

$$I_{avg} = \frac{I_{peak} - I_{bot}}{2} \quad (1),$$

where L is the grid-tied inductor. The increase in inductor current ΔI_L during the Mode 1 output time T_{on} is expressed by

$$\Delta I_L = I_{peak} + I_{bot} = \frac{V_{in} - v_c}{L} T_{on} \quad (2).$$

Based on (1) and (2), the required on-time T_{on} to get the desired average current is derived in

$$T_{on} = 2L \frac{I_{avg} + I_{bot}}{V_{in} - v_c} \quad (3).$$

In conventional TCM control, the inverter outputs Mode 2 or 3 until the inductor current reaches I_{bot} without calculating the Mode 2 or 3 output time T_{off}. As a result, it is necessary to detect the instantaneous inductor current in real-time. This requires the current detection circuit to have a bandwidth significantly higher than the switching frequency. For this reason, the switching frequency in conventional methods is constrained by the bandwidth of the sensing circuit, which makes operation in the MHz range extremely challenging. The proposed method calculates the off-time T_{off} in advance to overcome this limitation. The decrease in inductor current during Mode 2 or 3 is expressed by

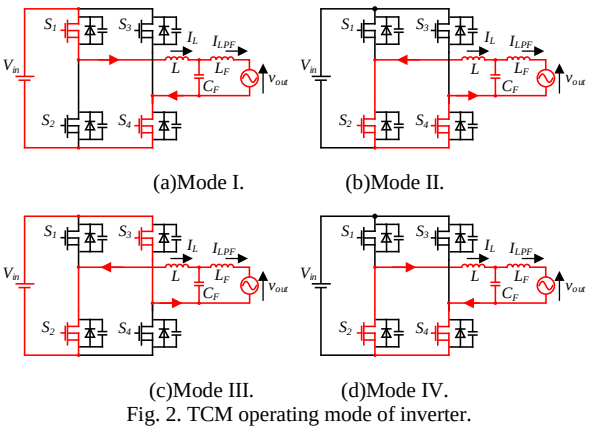

Fig. 2. TCM operating mode of inverter.

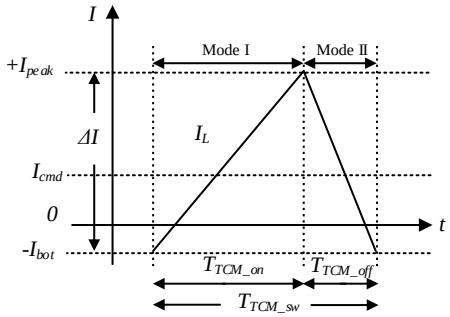

(a) I_L of positive output polarity.

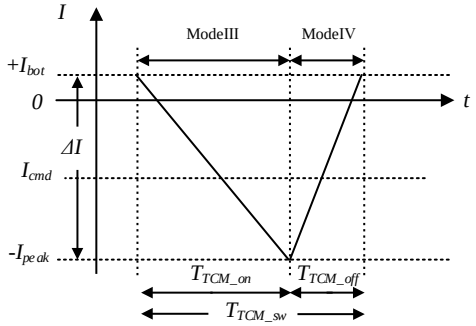

(b) I_L of negative output polarity.

Fig. 3. Inductor current waveform of TCM.

$$\Delta I_L = I_{peak} + I_{bot} = \frac{v_{out}}{L} T_{off} \quad (4),$$

Accordingly, the off-time Toff is derived as (5) from (1) and (4).

$$T_{off} = 2L \frac{I_{avg} + I_{bot}}{v_c} \quad (5).$$

Figure 4 shows a block diagram for compensating inductor current error. Errors may occur in the grid-tied inductor current when T_{on} and T_{off} are calculated from (3) and (5) without bottom current detection. These errors occur because the desired peak current I_{peak} and bottom current I_{bot} cannot be accurately achieved due to parameter deviations in the grid-tied inductor and fluctuations in the input and output voltages. The feedback control compensates for the inductor current error by using the filter inductor current with the ripple removed. It enables the use of conventional current sensors. As a result, the sampling period can be longer than the switching period.

C. Design of inductors

The inductance of the grid-tied inductor determines the switching frequency in TCM control. In this paper, the inductance is designed based on the minimum switching frequency under rated operation. The switching frequency is the sum of the on-time T_{on} and the off-time T_{off}, which is expressed by

$$f_{sw} = \frac{1}{T_{off} + T_{on}} = \frac{v_{out}}{2L\left(I_{avg} + I_{bot}\right)}\left(1 - \frac{v_{out}}{V_{in}}\right) \quad (6).$$

According to (6), the switching frequency reaches its minimum when the voltage applied to the inductor is at its maximum. Thus, the grid-tied inductance is calculated by

$$L = \frac{V_{\max}}{2 f_{\min}\left(I_{\max} + I_{bot}\right)}\left(1 - \frac{V_{\max}}{V_{in}}\right) \quad (7),$$

where I_{max} is the maximum current and V_{max} is the maximum voltage.

III. Simulation Result

Table 1 shows the simulation conditions, and Figure 5 presents the resulting waveforms. The minimum switching frequency in the simulation is set to 2 MHz to avoid interference with AM radio, which operates up to 1.6 MHz. In addition, the feedback of the filter inductor current is turned off partway through the simulation. Figure 5 shows that the grid-tied inductor current operates in TCM under the proposed control method and the bottom current remains constant. Furthermore, the output current is significantly distorted when the feedback control is disabled, which confirms the effectiveness of the feedback control.

IV. Experimental Result

Table 2 shows the experimental conditions. The experiment uses a mini model with a minimum switching frequency of 100 kHz. A 100 Ω resistive load is used.

Figure 6 shows the operating waveform when the feedback control is disabled. Figure 7 presents an enlarged waveform around the peak current in Figure 6. The experimental results indicate that the output current is significantly distorted and the negative current is not constant.

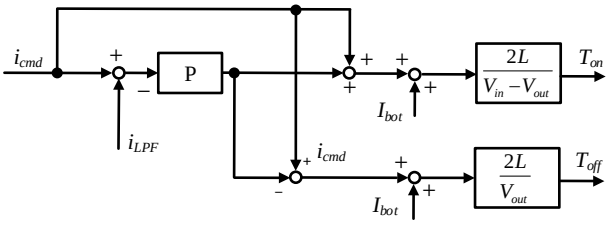

Fig. 4. Block diagram of I_L error compensation.

Table 1. Simulation Parameters.

Simulation conditions	Value
Input voltage V_{in}	400 V
Output voltage V_{out}	200 V_{RMS}
Output Command Current I_{cmd}	5 A_{RMS}
Grid connect inductor L	2.85 µH
Switching minimum frequency f_{sw_min}	2 MHz
Filter inductor L_f	2.53 mH
Filter capacitor C_f	1.0 nF
Bottom current I_{bot}	800 mA

Table 2. Experiment Parameters.

Experimental conditions	Value
Input voltage V_{in}	200 V
Output voltage V_{out}	100 V_{RMS}
Output Command Current I_{cmd}	1 A_{RMS}
Grid connect inductor L	127.66 µH
Switching minimum frequency f_{sw_min}	100 kHz
Filter inductor L_f	1.7 mH
Filter capacitor C_f	6.6 µF
Bottom current I_{bot}	200 mA

Compared to the simulation, the distortion is reduced due to using a resistive load. Figure 7 also confirms that ZVS is achieved. However, since the bottom current is not constant, it implies that a large amount of unnecessary current is flowing.

Figure 8 shows the waveform when the feedback control is applied. Figure 9 presents an enlarged waveform at the peak current in Figure 8. The experimental results show that the output current is sinusoidal and the bottom current remains constant. The total harmonic distortion (THD) of the output current is 2.8%. In addition, Figure 9 confirms that ZVS is achieved. However, distortion is observed in the filter inductor current near the zero-crossing point. This distortion occurs because the output voltage becomes nearly zero at the zero-crossing, which makes it difficult to fully discharge the

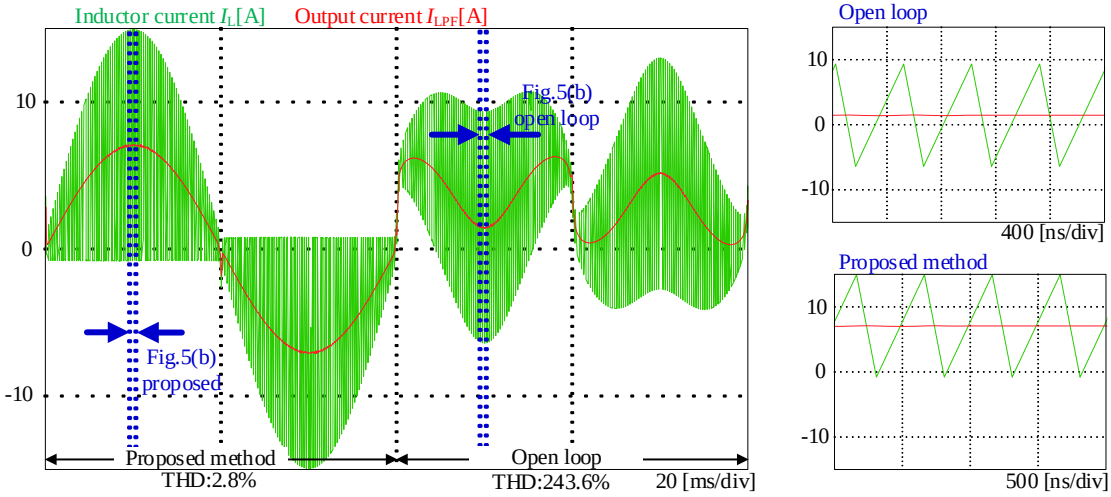

(a) Output Waveform (b) Enlarged output current waveform

Fig. 5. Operating waveform with the proposed method.

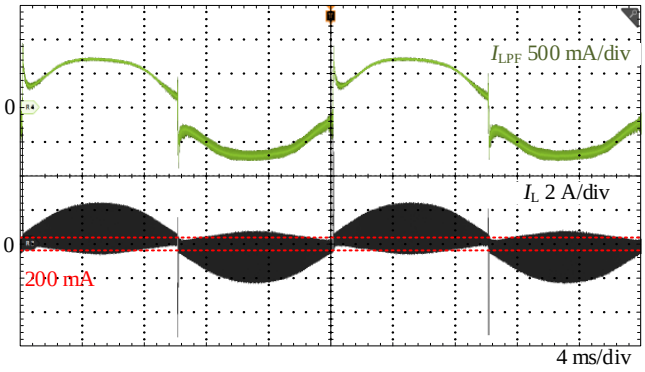

Fig. 6. Experiment waveform of TCM open loop.

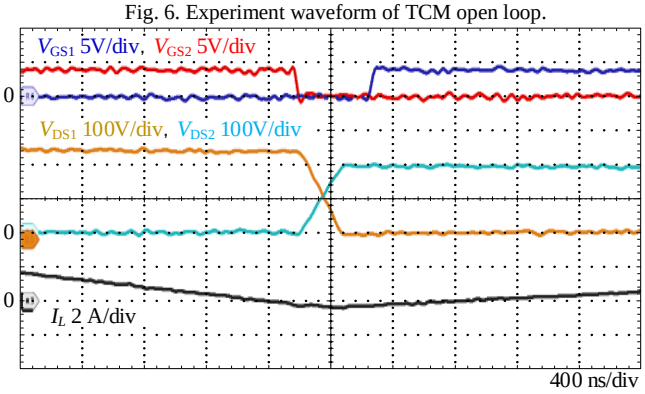

Fig. 7. Enlarged waveform of TCM open loop.

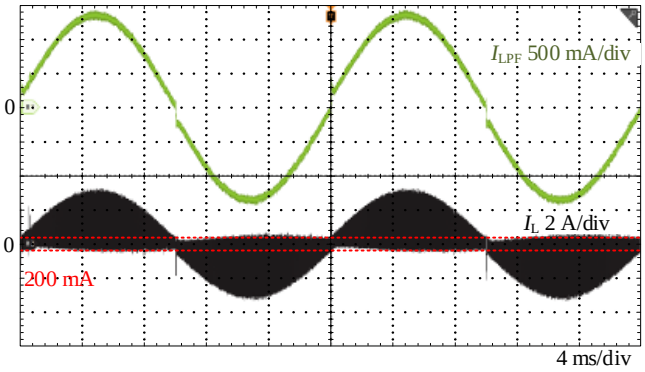

Fig. 8 Current waveform of the proposed method.

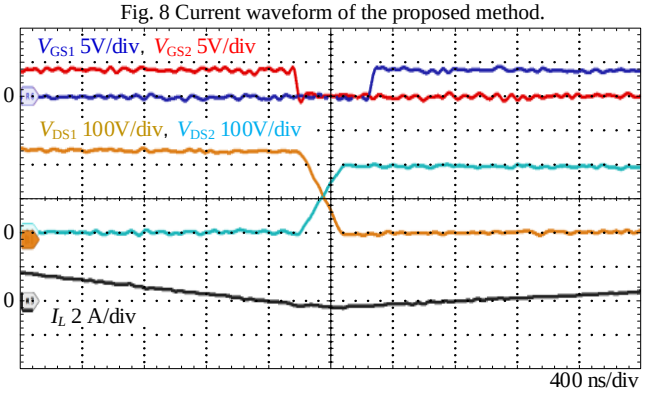

Fig. 9. Enlarged waveform of the proposed method.

inductor current. For this reason, near the zero-crossing point, it is necessary to either switch to DCM operation or apply a switching pattern that enables complete inductor current discharge.

V. Conclusion

This paper proposes a control method for a full-bridge inverter that operates above 2 MHz, aiming to achieve higher power density in the USPM. The proposed method employs a triangular current mode (TCM) without detecting the bottom current using a shunt resistor. The proposed method calculates the turn-on and turn-off times of the switching devices, allowing the system to operate without the need for high-speed current detection. In addition, low-speed current detection and feedback control compensate for current errors caused by input/output voltage disturbances. The effectiveness of the proposed method is verified through both simulation and experiment. The experimental results confirm that the proposed control method enables TCM operation without bottom current detection. Furthermore, the total harmonic distortion (THD) of the output current is measured to be 2.8% under the proposed control. Future work includes improving the distortion near the zero-crossing point and conducting experiments at a minimum switching frequency of 2 MHz to avoid interference with AM radio.

Acknowledgment

The Council for Science, Technology and Innovation(CSTI), Cross-ministerial Strategic Innovation Promotion Program (SIP) supported this work.

References

[1] T. Kitamura, M. Yamada, S. Harada, and M. Koyama, "Development of high-power-density interleaved DC/DC converter with SiC devices," IEEJ Trans. Ind. Appl., vol. 134, no. 11, pp. 956–961, 2015.

[2] K. Yamanokuchi, H. Watanabe, and Jun-ichi Itoh, "Droop-based current control method in autonomous distributed modular power conversion system," in Proc. IEEE Appl. Power Electron. Conf. Expo. (APEC), Phoenix, AZ, USA, 2021, pp. 660–667.

[3] K. Yamanokuchi, H. Watanabe, and Jun-ichi Itoh, "Distributed control method for power conversion system with series-connected autonomous modular converters," IEEE Trans. Power Electron., vol. 38, no. 12, pp. 15242–15252, 2023.

[4] D. Hiroe, X. Zhang, K. Nakamura, K. Sato, R. Suzuki, K. Yoshimoto, and T. Yokoyama, "A study of 10 MHz multi-sampling deadbeat control for PMSM drive system using USPM controller," IEEJ J. Ind. Appl., vol. 12, no. 3, pp. 508–516, 2023.

[5] K. Yamanokuchi, H. Watanabe, and Jun-ichi Itoh, "Universal smart power module concept with high-speed controller for simplification of power conversion system design," in Proc. IEEE 12th Energy Convers. Congr. Expo. - Asia (ECCE-Asia), Singapore, 2021, pp. 2484–2489.

[6] H. Watanabe, K. Yamanokuchi, Y. Ikeda, Y. Takahashi, and Jun-ichi Itoh, "Universal smart power module (USPM) for carbon neutral society," IEEE Trans. Ind. Appl., vol. 60, no. 2, pp. 3411–3417, 2024.

[7] M. Sakamoto and H. Haga, "Control method for universal smart power module considering wireless communication," IEEJ J. Ind. Appl., vol. 12, no. 2, pp. 204–214, 2023.

[8] D. Yamanodera, R. Iijima, T. Isobe, and H. Tadano, "Experimental verification and loss analysis of MHz-operating discontinuous current-mode grid-tied inverter using GaN-HEMT device," IEEJ Trans. Ind. Appl., vol. 139, no. 3, pp. 249–257, 2019.

[9] Y. Lei, C. Barth, S. Qin, W. Liu, I. Moon, A. Stillwell, D. Chou, T. Foulkes, Z. Ye, Z. Liao, and R. C. N. Pilawa-Podgurski, "A 2 kW, single-phase, 7-level, GaN inverter with an active energy buffer achieving 216 W/in³ power density and 97.6% peak efficiency," in Proc. IEEE Appl. Power Electron. Conf. Expo. (APEC), Long Beach, CA, USA, 2016, pp. 1512–1519.

[10] C. Marxgut, F. Krismer, D. Bortis, and J. W. Kolar, "Ultraflat interleaved triangular current mode (TCM) single-phase PFC rectifier," IEEE Trans. Power Electron., vol. 29, no. 2, pp. 873–882, 2014.

[11] D. P. Nguyen, Y.-C. Liu, X.-R. Chen, and H.-J. Chiu, "GaN-based interleaved four-level flying capacitor triangular conduction mode (TCM) converter with coupled inductors," IEEJ J. Ind. Appl., vol. 13, no. 6, pp. 645–654, 2024.